Synthesis and Structure–Conductivity Relationship of Polystyrene-*block*-Poly(vinyl benzyl trimethylammonium) for Alkaline Anion Exchange Membrane Fuel Cells

Tsung-Han Tsai,[1] Ashley M. Maes,[2] Melissa A. Vandiver,[2] Craig Versek,[3] Sönke Seifert,[4] Mark Tuominen,[3] Matthew W. Liberatore,[2] Andrew M. Herring,[2] E. Bryan Coughlin[1]

[1]Department of Polymer Science and Engineering, University of Massachusetts Amherst, 120 Governors Drive, Amherst, Massachusetts 01003

[2]Department of Chemical and Biological Engineering, Colorado School of Mines, Golden, Colorado 80401

[3]Department of Physics, University of Massachusetts Amherst, 411 Hasbrouck Laboratory, Amherst, Massachusetts 01003

[4]X-ray Science Division, Argonne National Laboratory, Argonne, Illinois 60439

Correspondence to: E. B. Coughlin (E-mail: coughlin@mail.pse.umass.edu)

Received 22 June 2012; accepted 17 August 2012; published online 21 September 2012
DOI: 10.1002/polb.23170

ABSTRACT: Block copolymers of polystyrene-*b*-poly(vinyl benzyl trimethylammonium tetrafluoroborate) (PS-*b*-[PVBTMA][BF_4]) were synthesized by sequential monomer addition using atom transfer radical polymerization. Membranes of the block copolymers were prepared by drop casting from dimethylformamide. Initial evaluation of the microphase separation in these PS-*b*-[PVBTMA][BF_4] materials via SAXS revealed the formation of spherical, cylindrical, and lamellar morphologies. Block copolymers of polystyrene-*b*-poly(vinyl benzyl trimethylammonium hydroxide) (PS-*b*-[PVBTMA][OH]) were prepared as polymeric alkaline anion exchange membranes materials by ion exchange from PS-*b*-[PVBTMA][BF_4] with hydroxide in order to investigate the relationship between morphology and ionic conductivity. Studies of humidity [relative humidity (RH)]-dependent conductivity at 80 °C showed that the conductivity increases with increasing humidity. Moreover, the investigation of the temperature-dependent conductivity at RH = 50, 70, and 90% showed a significant effect of grain boundaries in the membranes against the formation of continuous conductive channels, which is an important requirement for achieving high ion conductivity. © 2012 Wiley Periodicals, Inc. J. Polym. Sci., Part B: Polym. Phys. **2013**, *51*, 1751–1760

KEYWORDS: amphiphilic block copolymers; anion exchange membrane fuel cell; atom transfer radical polymerization (ATRP); phase separation; polymeric electrolyte membranes; polystyrene; poly(vinyl benzyl trimethylammonium); structure; conductivity relationship

INTRODUCTION Proton exchange membrane fuel cells (PEMFCs), which convert chemical energy to electrical energy through redox reactions, have been developed as renewable and portable energy devices because of their high efficiency, high energy density, and low formation of pollutants.[1,2] Commercially available Nafion®,[3] a perfluorosulfonic acid ionomer, has been widely investigated as a proton exchange membrane because of its good chemical stability, suitable mechanical properties, and high proton conductivity. However, because of the high cost of the membranes and their need for noble metal (i.e., platinum)-based electrocatalysts, the commercialization of PEMFCs is still limited. Additionally, oxygen reduction and fuel (hydrogen or alcohol) oxidation are sluggish under the acidic condition of cells, and the noble metal catalysts are easily poisoned by carbon monoxide at low temperature. These are serious obstacles to the extensive adoption of PEMFCs as energy devices.[4]

An alkaline fuel cell (AFC) uses potassium hydroxide as a liquid electrolyte.[5–9] When compared with PEMFCs, AFC conducts hydroxide ion from cathode to anode. The oxygen reduction[10] and fuel oxidation[11,12] are faster in alkaline condition than in acidic condition, allowing for the use of non-noble metal catalysts (i.e., nickel[13] and silver) and longer carbon chain alcohol fuels. Moreover, the corrosion of metal catalysts by carbon monoxide is reduced under the alkaline conditions of cells.[14] However, the use of potassium hydroxide solution results in leakage problems. The presence of carbon dioxide in hydrogen and air will react with potassium hydroxide to form potassium carbonate, which precipitates on the electrodes blocking the surface and reducing the efficiency of the cells. The use of alkaline anion exchange membrane (AAEM) with a suitable stable polymeric electrolyte can overcome the issues discussed above.[14–16] The requirements for a AAEM polymeric electrolyte are a robust

polymer backbone as well as an alkaline stable cationic charge to facilitate anion transport. An all-carbon polymer backbone will be hydrolytically stable. Benzyl trimethyl ammonium cations have proven to be stable under alkaline conditions because of the presence of steric hindrance and the absence of β-hydrogens preventing Hofmann elimination.[17]

Recently, Varcoe and coworkers[18–20] demonstrated radiation-grafted polyvinylidene fluoride, poly(ethylene-*co*-tetrafluoroethylene), and fluorinated ethylene propylene-containing polymeric benzyl trimethylammonium hydroxide ions for AAEMFCs. Additionally, chloromethylated polysulfones quaternized by treatment with trimethylamine are another class of AAEMFCs because of their good mechanical, thermal, and chemical stability.[21–23] Brominated benzylmethyl-containing polysulfones for AAEMFCs, as investigated by Yan and Hickner,[24] avoid the chloromethylation step, which is known to be a toxic and carcinogenic process. Cross-linked tetraalkylammonium-functionalized polyethylenes have been synthesized by ring-opening metathesis copolymerization of tetraalkylammonium-functionalized cyclooctenes with unfunctionalized cyclooctenes.[25] These crosslinked structures provide good mechanical properties and allow incorporation of higher proportion of ion conductive groups. Other crosslinked copolymers based on imidazolium and bis-imidazolium groups exhibited high hydroxide ion conductivity and good mechanical properties.[26,27] The incorporation of novel phosphonium cations with methoxyphenyl group into polysulfones was studied.[28] The electron-donating nature of oxygen in the phosphonium moieties stabilizes the cations, leading to good chemical durability under basic conditions. Guanidinium-functionalized poly(arylene ether sulfone) shows higher ion conductivity than trimethylammonium-functionalized polysulfone because of the higher basicity of guanidinium cation.[29] There is some question about the long-term stability of guanidinium cation under highly caustic conditions. Recently, base-stable benzimidazolium polymers designed with steric protection around the C2 position have been developed.[30] Solvent-processable polyfluorene ionomers containing pendant imidazolium moieties were investigated. These polyfluorene ionomer membranes show long-term stability under basic condition at elevated temperature, and hydroxide conductivity is above 10^{-2} S/cm at room temperature.[31] A random copolymer of poly(methyl methacrylate-*co*-butyl acrylate-*co*-vinylbenzyl chloride) was prepared and revealed the feasible preparation for the AAEM.[32] Different types of random copolymers with methyl methacrylate, vinylbenzyl chloride, and ethyl acrylate were fabricated as potential AAEMs for direct methanol AFC.[33] Till now, most of the studies on AAEM have been based on random copolymers containing cation conductive moieties.

The use of well-defined block copolymers with polycation as ionic conductive pathway can benefit the investigation of the relationship between structure and ionic conductivity of the membranes. Microphase separation in block copolymers can provide a versatile platform for the fabrication of nanostructured materials with a wide range of morphologies depending on the segregation strength (χ) and the degree of polymerization (N)-accessible structures include cylinders, lamellas, and gyroids.[34,35] Polymeric conductive membranes made from block copolymers can provide well-oriented and continuous conductive hydrophilic channels to enhance ion conductivity. Because of the presence of the hydrophobic domain in the membranes, the mechanical property of the membranes can also be enhanced. Therefore, more ion conductive groups can be incorporated into the polyelectrolyte leading to higher conductivity [higher ion exchange capacity (IEC) $>$ 1.5 mequiv/g]. In contrast to random copolymers, it is difficult to achieve higher IEC because of the swelling encountered at high states of hydration leading to disintegration of the membranes. Several studies about structure–morphology–property relationships of block copolymers for PEM have shown that the morphology of the conductive membranes strongly influences their proton conductivity on the aspect of type and orientation of structure.[36–42] Till now, fundamental investigations about the relationship between morphology and conductivity in AAEM made from well-defined block copolymers are sparse. The block copolymers poly(arylene ether)s containing ammonium-functionalized fluorene groups explored by Watanabe et al.[43] show high IEC up to 1.93 mequiv/g and high conductivity (144 mS/cm) at 80 °C. The membrane is mechanically and chemically stable, similar to the membranes from random copolymers. Therefore, using block copolymers with hydrophilic blocks could improve the ionic conductivity of AEM by incorporating more conductive group without losing mechanical properties.

In the current investigations, we have synthesized block copolymers of polystyrene-*b*-poly(vinyl benzyl trimethylammonium tetrafluoroborate) (PS-*b*-[PVBTMA][BF_4]) via sequential monomer addition using atom transfer radical polymerization (ATRP) without the need to perform any post-polymerization modification. The membranes of PS-*b*-[PVBTMA][BF_4] diblock copolymers were readily prepared via solvent-casting. Polystyrene-*b*-poly(vinyl benzyl trimethylammonium hydroxide) (PS-*b*-[PVBTMA][OH]) was subsequently prepared by ion exchange with potassium hydroxide to produce the AAEMFC materials. The morphology of the membranes of PS-*b*-[PVBTMA][BF_4] and PS-*b*-[PVBTMA][OH] block copolymers was determined by small-angle X-ray scattering (SAXS) at different humidity and temperature conditions. The effects of the morphologies on the ionic conductivity, measured by impedance spectroscopy, were also investigated.

EXPERIMENTAL

Materials

Styrene (>99%; Aldrich) was passed through a column of basic alumina. Anhydrous *N, N*-dimethylformamide (DMF, 99.8%; Alfa Aesar), vinyl benzyl trimethylammonium chloride ([VBTMA][Cl], 99%; Aldrich), sodium tetrafluoroborate ($NaBF_4$, 97%; Alfa Aesar), copper(I) bromide (CuBr, 99.999%; Aldrich), (1-bromoethyl)benzene (97%; Alfa Aesar), and 1,1,4,7,10,10-hexamethyltriethylenetetramine (HMTETA, 97%; Aldrich) were used as received. All solvents were of ACS grade.

Characterizations

^{1}H NMR spectroscopy was performed on a Bruker DPX-300 FT-NMR. Gel permeation chromatography (GPC) was

performed in tetrahydrofuran (THF) on a Polymer Laboratories PL-GPC 50 Integrated GPC system. Infrared spectroscopy was performed on a Perkin-Elmer 100 FTIR spectrometer with universal ATR sampling accessory. SAXS experiments were performed on beamline 12 ID-B at The Basic Energy Sciences Synchrotron Radiation Center at the Advanced Photon Source at Argonne National Laboratory. A Pliatus 2M SAXS detector was used to collect scattering data with an exposure time of 1 s. The X-ray beam had a wavelength of 1 Å and power of 12 keV. The intensity (I) is a radial integration of the 2D scattering pattern with respect to the scattering vector (q).

Temperature and humidity were controlled within a custom sample oven. Typical experiments studied three membrane samples and one empty window so that a background spectrum of the scattering through just the Kapton windows and nitrogen environment could be obtained for each experimental condition. The humidity of the sample environment was controlled by mixing heated streams of saturated and dry nitrogen. Sample holders were inserted into an oven environment of 40 °C and 50% relative humidity (RH). The samples were allowed to take up water for 20 min before X-ray spectra were taken. A 50% RH was maintained as the temperature was then increased to 50 °C and then to 60 °C. The spectra were taken 20 min after the temperature set points were changed. Temperature was then maintained at 60 °C while the RH was stepped up to 75% and then to 95% with 15-min steps.

Conductivity Measurement

Ionic conductivity measurements were made by using impedance spectroscopy using custom electrode assemblies and automation software within the humidity- and temperature-controlled environment of an ESPEC SH-241 test chamber. The free-standing membrane samples of irregular areas were lightly compressed between two gold-plated stainless steel electrodes, the top having an area of $A = 0.07917$ cm^2 (1/8 inch diameter) and bottom having a 1/2 inch diameter, such that there was exposed material on the top surface. The impedance spectra were sampled at regular intervals of 20 min using a Solartron 1260 Impedance/Gain Phase Analyzer over a range of 10 MHz to 0.1 Hz in logarithmic steps of 10 points per decade; the portion of each spectrum forming a "plateau" in the impedance magnitude and corresponding to the first local phase minimum nearest the low-frequency range was fitted to a constant magnitude function and interpreted as the bulk resistance R to ion transport within the membrane. The thickness t of each membrane was measured with a micrometer and the effective area for the conductance measurement was estimated as the area of the smaller top electrode A so that conductivity was computed as conductivity (σ) $= t/(A \times R)$. The thickness of the membranes is 189, 242, and 310 μm for PS-*b*-[PVBTMA][BF_4]-1, -2, and -3, respectively.

Ion Exchange of [VBTMA][BF_4]

The ion exchange of [VBTMA][Cl] was performed as previously reported.[44] [VBTMA][Cl] (2.2 g, 10.39 mmol) and $NaBF_4$ (1.255 g, 11.43 mmol) were dissolved in 200 mL of acetonitrile and stirred at ambient temperature overnight. The solution was filtered, and the filtrate was concentrated. White crystals were obtained by precipitation in anhydrous diethyl ether and then dried in vacuum at 40 °C.

Synthesis of [PVBTMA][BF_4] by ATRP

Nitrogen-purged DMF (2 mL), (1-bromoethyl)benzene (7.03 mg, 0.038 mmol), and HMTETA (8.75 mg, 0.038 mmol) were added to a Schlenk tube containing a mixture of [VBTMA][BF_4] (1 g, 3.8 mmol) and CuBr (5.45 mg, 0.038 mmol). The mixture was put under vacuum and refilled with nitrogen three times. The mixture was degassed by three freeze-pump-thaw cycles followed by stirring at 90 °C. Aliquot samples were taken and analyzed to determine conversion of the reaction by ^{1}H NMR.

Synthesis of Polystyrene (PS-Br) by ATRP

The polymerization of styrene was performed as reported in the literature.[45] Styrene (36.36 g, 348.8 mmol) was added to a Schlenk tube containing a mixture of CuBr (74.5 mg, 0.519 mmol), (1-bromoethyl)benzene (99.0 mg, 0.519 mmol), and HMTETA (119.6 mg, 0.519 mmol). The mixture was degassed by three freeze-pump-thaw cycles followed by stirring at 110 °C for 5 h. After polymerization, the reaction solution was quenched in an ice bath, then passed through a pad of basic alumina to remove the copper catalyst, and precipitated in methanol three times to obtain polystyrene as a white powder.

Synthesis of PS-b-[PVBTMA][BF_4] by ATRP

Nitrogen-purged DMF (4 mL) and HMTETA (4.6 mg, 0.05 mmol) were added to a Schlenk tube containing a mixture of PS-Br (700 mg, $M_n = 35$ kg/mol), [VBTMA][BF_4] (700 mg, 2.67 mmol), and CuBr (2.86 mg, 0.02 mmol). The mixture was degassed by three freeze-pump-thaw cycles followed by stirring at 90 °C. The polymer was precipitated into methanol.

Preparation of PS-b-[PVBTMA][BF_4] Membranes

PS-*b*-[PVBTMA][BF_4] membranes were drop cast from DMF (10 wt % solution) onto a Teflon sheet. The membranes were first dried at ambient temperature for 7 days and then under vacuum at 40 °C.

Ion Exchange of PS-b-[PVBTMA][OH]

PS-*b*-[PVBTMA][BF_4] membranes were soaked in 1 M KOH aqueous solution for 3 days. The solution was changed several times, and then the membranes were immersed in water for 1 day.

Water Uptake

The PS-*b*-[PVBTMA][OH] membranes were soaked into the deionized water at room temperature for 24 h. The weight of hydrated membranes (W_{wet}) was measured after wiping the excess water on the surface. The weight of dry membrane (W_{dry}) was obtained by drying the wet membranes under vacuum at 60 °C. The water uptake was calculated using the following equation:

$$\text{Wateruptake} = \frac{W_{wet} - W_{dry}}{W_{dry}} \times 100\% \quad (1)$$

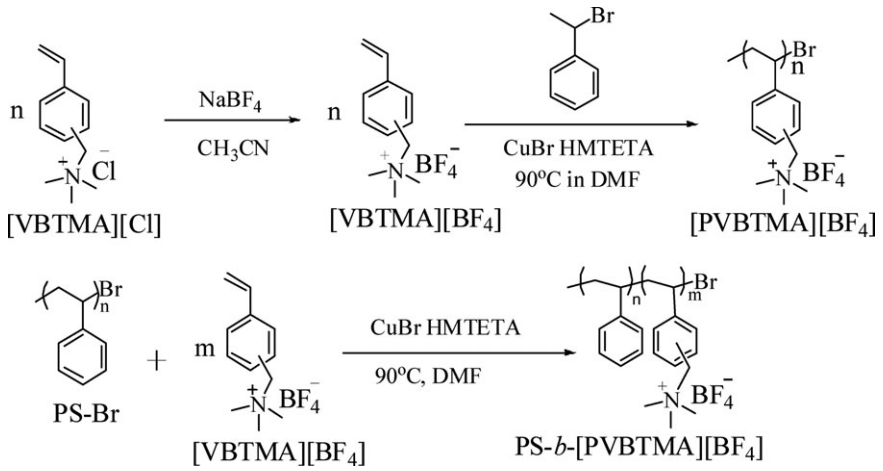

SCHEME 1 Synthesis of poly(vinyl benzyl trimethylammonium tetrafluoroborate) [PVBTMA][BF_4] homopolymers and polystyrene-*b*-poly(vinyl benzyl trimethylammonium tetrafluoroborate) PS-*b*-[PVBTMA][BF_4] block copolymers.

RESULTS AND DISCUSSION

Synthesis of PS-b-[PVBTMA][BF_4] and PS-b-[PVBTMA][OH]

Amphiphilic block copolymers of polystyrene-*b*-poly(vinyl benzyl trimethylammonium) (PS-*b*-[PVBTMA]) have been synthesized by quaternization with trimethylamine to the block copolymers polystyrene-*b*-polyvinyl benzyl chloride that have already been synthesized by sequential stable free-radical polymerization[46] or reversible addition fragmentation transfer.[47] In this study, block copolymers PS-*b*-[PVBTMA][BF_4] were synthesized directly by sequential ATRP without the need for any postchemical modification. First, the ATRP of [PVBTMA][BF_4] was investigated to confirm its living character. As shown in Scheme 1, [VBTMA][BF_4] was prepared by ion exchange from commercially available [VBTMA][Cl] with $NaBF_4$.[44] Because of the ion exchange, this monomer became slightly less hydrophilic and was soluble in DMF. The polymerization of [VBTMA][BF_4] was achieved via ATRP catalyzed by a CuBr/HMTETA complex at 90 °C in DMF. The linear increase of conversion versus time (shown in Fig. 1) was observed when the conversion was kept below 50%. Conversion reaches a plateau at 50% probably due to the poor solubility of the polymer chains in the reaction mixture. DMF is also a solvent for polystyrene. Therefore, block copolymer PS-*b*-[PVBTMA][BF_4] can be directly synthesized by ATRP in DMF without any postchemical modification.

The synthetic route for PS-*b*-[PVBTMA][BF_4] is shown in Scheme 1. The macroinitiator PS-Br with M_n = 35 kg/mol and dispersity ($Đ$) = 1.13 was synthesized via ATRP catalyzed by a CuBr/HMTETA complex. PS-*b*-[PVBTMA][BF_4] materials were then synthesized by ATRP of [VBTMA][BF_4] using the PS-Br as macroinitiator in DMF at 90 °C. After the copolymerization, aliquots of solution were analyzed by ^{1}H NMR in DMSO-d_6 to measure the conversion. The conversion of the copolymerization was also analyzed by yield measurements to confirm the progress of copolymerization. PS-*b*-[PVBTMA][BF_4]-*x* are summarized in Table 1, where *x* refers to the theoretical IEC based on the conversion calculated by ^{1}H NMR. The $Đ$ and M_n of the resulting block copolymers cannot be measured directly by GPC due to lack of a suitable solvent system to serve as the eluent. The M_n of the [PVBTMA][BF_4] was calculated based on the conversion measurements. The conversion analyzed by yield was typically lower than that measured by ^{1}H NMR because of the loss of product during precipitation and collection. Therefore, the composition and IEC of the block copolymers were based on the conversion calculated by ^{1}H NMR.

Membranes of the PS-*b*-[PVBTMA][BF_4] were made by drop casting from DMF. To determine the conversion of anion exchange, these membranes were characterized by FTIR. Figure 2 shows the FTIR spectrum of PS-*b*-[PVBTMA][BF_4] before and after ion exchange in 1 M KOH aqueous solution for 3 days in a sealed vial. The disappearance of the characteristics band at 1048 cm^{-1} corresponding to the

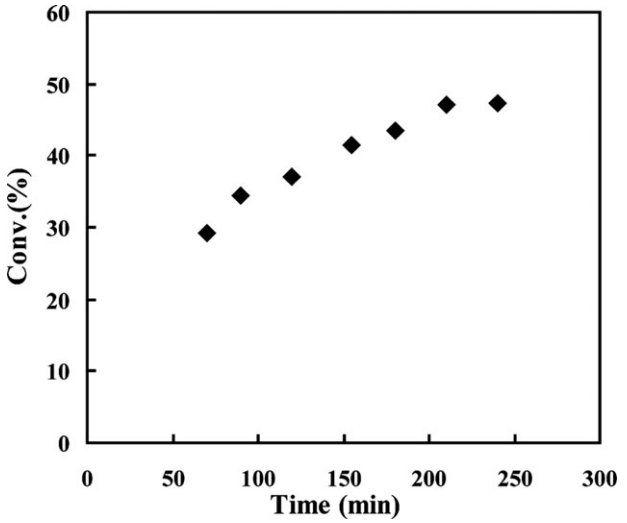

FIGURE 1 Time dependence of conversion for polymerization of [VBTMA][BF_4] by ATRP. $[[VBTMA][BF_4]]_0/[initiator]_0/[CuBr]_0/[HMTETA]_0$ = 100:1:1:1 and [VBTMA][BF_4] = 1.9 M.

TABLE 1 Samples of PS-*b*-[PVBTMA][BF_4]

PS-*b*-[PVBTMA][BF_4]-*x*	Conv.[a] [(%)$_{NMR}$]	Conv.[b] [(%)$_{Yield}$]	$M_{n,\ NMR}$ of [PVBTMA][BF_4][c] (g/mol)	$M_{n,\ Yield}$ of [PVBTMA][BF_4][d] (g/mol)	PS[e] [mole(%)$_{NMR}$]	Water Uptake[f] (%)	IEC[g] [(mequiv/g)$_{NMR}$]
PS-*b*-[PVBTMA][BF_4]-1.36	56.2	44.1	19,600	15,500	64	38.6	1.36
PS-*b*-[PVBTMA][BF_4]-1.19	35.7	28.2	16,100	12,700	68	25.0	1.19
PS-*b*-[PVBTMA][BF_4]-0.58	15.7	15.1	6,300	6,100	84	9.2	0.58

[a] The conversion was calculated by ^{1}H NMR spectra of reaction mixture after copolymerization in DMSO-d_6.
[b] The conversion was calculated by the yield of copolymerization.
[c] M_n of [PVBTMA][BF_4] was determined by the conversion from ^{1}H NMR after copolymerization.
[d] M_n of [PVBTMA][BF_4] was calculated by the conversion obtained from the yield of the copolymerization.
[e] The mole ratio of PS to [PVBTMA][BF_4] was calculated from ^{1}H NMR.
[f] Water uptake was measured with hydroxide anion at room temperature.
[g] Ion exchange capacity (IEC) of the samples are calculated from the composition ratio between PS and [PVBTMA][BF_4].

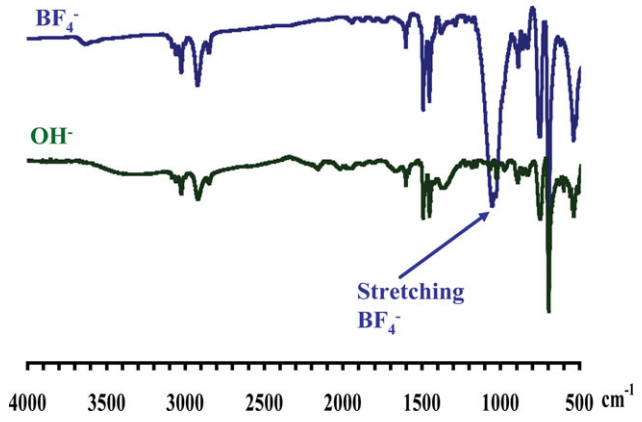

FIGURE 2 FTIR spectra of the PS-*b*-[PVBTMA][BF_4]-1.19 membrane (upper trace) and the PS-*b*-[PVBTMA][OH]-1.19 membrane (lower trace).

tetrafluoroborate anion and the presence of the characteristic signal of hydroxide anion (O—H stretching at around 3500 cm^{-1}) indicate complete ion exchange.

Morphology Studies on the PS-b-[PVBTMA][BF_4] and PS-b-[PVBTMA][OH] by SAXS

Originally, the membranes of the PS-*b*-[PVBTMA][BF_4] were made by drop casting from dichloromethane (DCM), chloroform, THF, or DMF. SAXS experiments were performed at room temperature to determine the self-assembly behavior these of PS-*b*-[PVBTMA][BF_4] membranes. SAXS data [log(*I*) vs. *q*] for the membranes cast from the different solvents show that the morphology of the membranes cast from DMF, a good solvent for both blocks, shows a lower degree of order. On the contrary, SAXS data for the membranes cast from DCM, a selective solvent for the PS, showed distinct higher order peaks. Therefore, well-defined morphologies of the membrane can be obtained by choosing a selective solvent from which to drop cast membranes. However, attempts

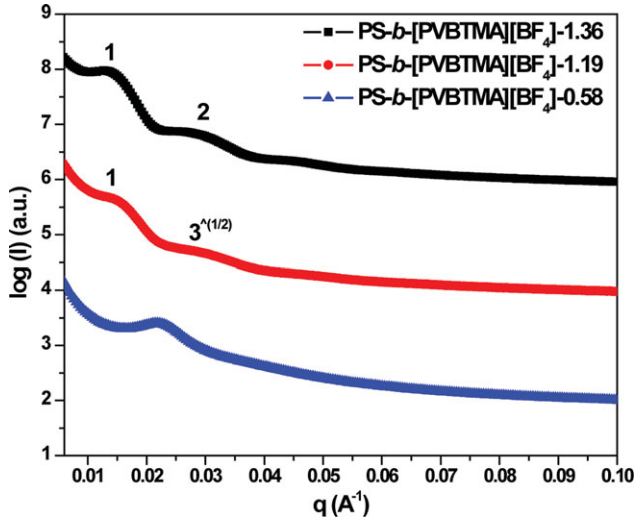

FIGURE 3 SAXS profiles of PS-*b*-[PVBTMA][BF_4] membranes drop cast from DMF.

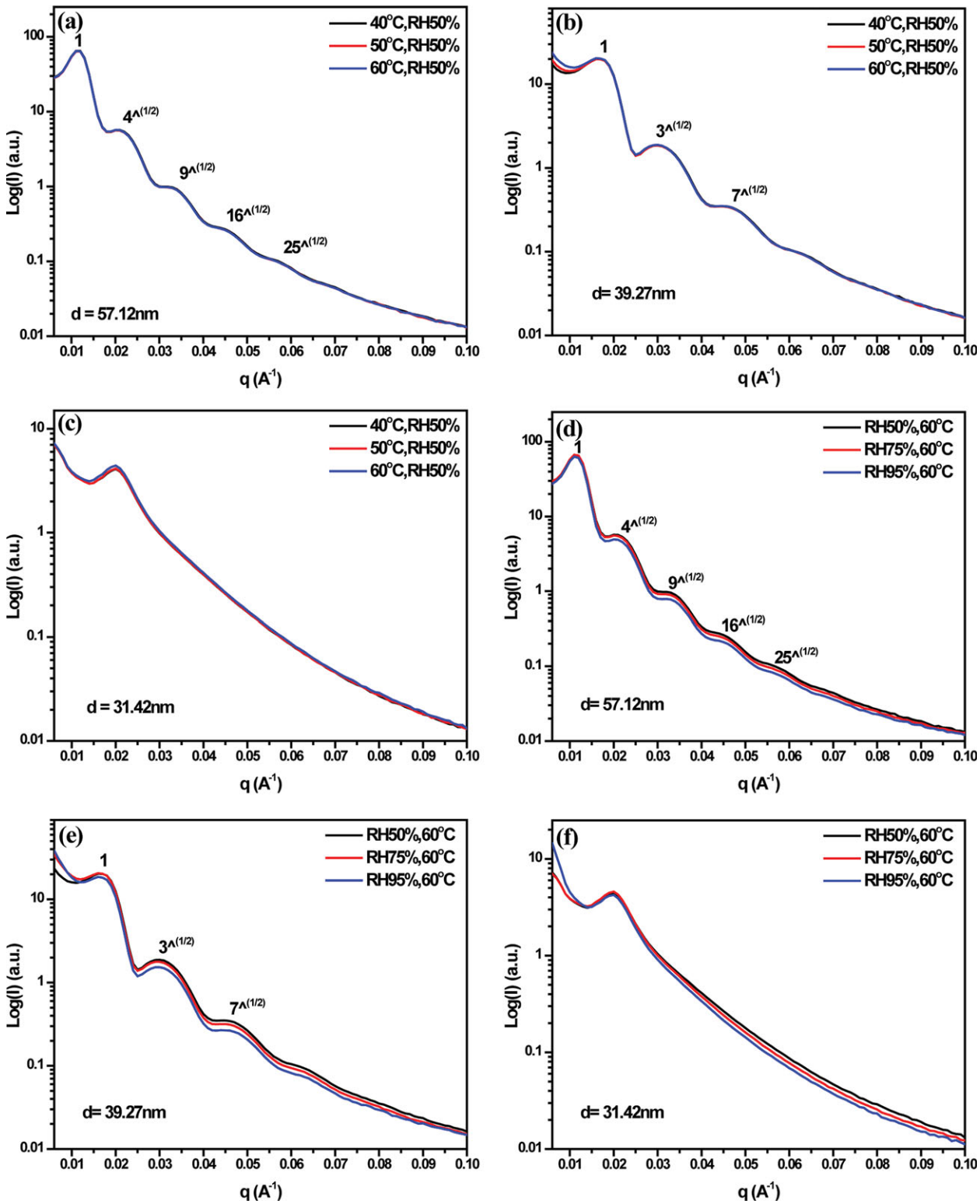

FIGURE 4 SAXS profiles of PS-*b*-[PVBTMA][OH] membranes cast from DMF. (a) PS-*b*-[PVBTMA][OH]-1.36; (b) PS-*b*-[PVBTMA][OH]-1.19; and (c) PS-*b*-[PVBTMA][OH]-0.58 at 50% RH with increasing temperature from 40 to 60 °C. (d) PS-*b*-[PVBTMA][OH]-1.36; (e) PS-*b*-[PVBTMA][OH]-1.19; and (f) PS-*b*-[PVBTMA][OH]-0.58 at 60 °C with 50, 75, and 95% RH.

to perform ion exchange to hydroxide anion for the membranes drop cast from DCM were not successful, as judged by FTIR analysis, likely due to the formation of a micelle-like structures with PS as corona and [PVBTMA][BF_4] as core in DCM, disturbing the formation of continuous ion-conductive channels when drop casting the membranes from DCM.

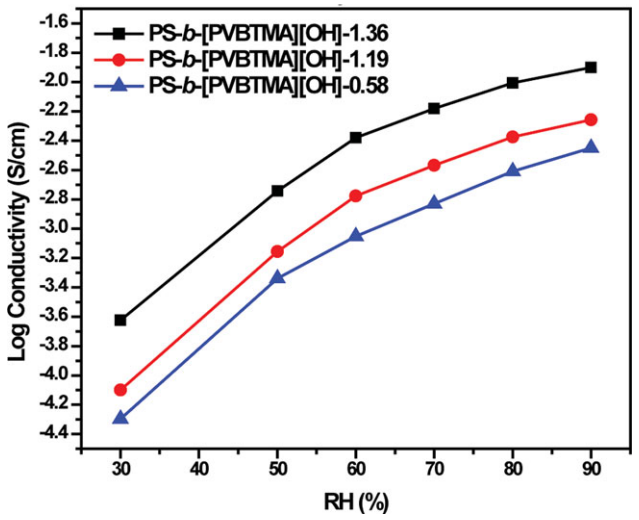

FIGURE 5 Humidity (RH)-dependent conductivity for PS-*b*-[PVBTMA][OH] membranes at 80 °C.

Membranes drop cast from DMF, while less ordered as shown by SAXS analysis, undergo successful conversion to the hydroxide counter ion. SAXS data of different PS-*b*-[PVBTMA][BF_4] samples drop cast from DMF are shown in Figure 3. For PS-*b*-[PVBTMA][BF_4]-1.36, the SAXS data show two scattering peaks at q* and 2q*, and therefore, it likely forms a lamellar structure. For PS-*b*-[PVBTMA][BF_4]-1.19, the appearance of two scattering peaks at q* and $3^{(1/2)}$q* indicates a cylindrical morphology. Only one peak for PS-*b*-[PVBTMA][BF_4]-0.58 is observed by SAXS, and thus, these data are not sufficient to distinguish the morphology. From the decreasing volume fraction of [PVBTMA][BF_4], it likely forms a spherical morphology.

The morphology of PS-*b*-[PVBTMA][OH] membranes was determined by SAXS at a fixed RH at 50% with increasing temperature from 40 to 60 °C and at a fixed temperature of 60 °C with different RHs at 50, 75, and 95% (shown in Fig. 4). For PS-*b*-[PVBTMA][OH]-1.36, the SAXS data [Fig. 4(a, d)] showing scattering peaks at q* and 2q*, 3q*, 4q*, and 5q* indicate that its microphase separates into a lamellar structure with long-range order. The SAXS data of PS-*b*-[PVBTMA][OH]-1.19 show reflections at q*, $3^{(1/2)}$q*, and $7^{(1/2)}$q*, exhibiting a cylindrical morphology [Fig. 4(b, e)]. When compared with the SAXS data with BF_4^-, the increase of peak intensity and the appearance of high-order peaks are due to the swelling by water enhancing the scattering contrast. From the SAXS data, only one peak is seen for PS-*b*-[PVBTMA][OH]-0.58 due to the lack of long-range order [Fig. 4(c, f)]. From the decreasing of [PVBTMA][OH] content, it presumably is a spherical morphology. The SAXS data for these three membranes at RH at 50% with increasing temperature from 40 to 60 °C and at 60 °C with different RH at 50, 75, and 95% demonstrate that no significant phase transition happens during changing the environmental condition. The polystyrene ($T_g \sim 100$ °C) as the hydrophobic domain can confine any structural expansion and contraction of PS-*b*-[PVBTMA][OH] membranes as the humidity is raised or lowered.

Morphology–Conductivity Relationships at Fixed Temperature with Increasing RH

The humidity-dependent conductivity of PS-*b*-[PVBTMA][OH] membranes at 80 °C is shown in Figure 5. From the log conductivity versus humidity plot, the conductivity systematically increases with increasing humidity for all three samples because the water uptake in the membrane facilitates ion conduction. Additionally, the conductivity increases with increasing IEC of the materials; however, it does not increase proportionally. The conductivity increases from 0.36–5.53 mS/cm to 12.55 mS/cm at RH = 90% and 80 °C when IEC changes from 0.58–1.19 mequiv/g to 1.36 mequiv/g. This unexpected relationship between conductivity and IEC may result from the inherent nature of the microstructures in these materials. Balsara and coworkers[48] proposed a morphology factor for block copolymers containing one ionic blocks with anisotropic-oriented structures, *f*:

$$\sigma = f\phi_c\sigma_c \tag{2}$$

where σ is the measured conductivity, and ϕ_c and σ_c are the volume fraction and intrinsic conductivity of the conducting block, respectively.

Sax and Ottino suggested that a factor of two-thirds be applied to ion transport in a lamellar structure ($f = 2/3$).[49] Following similar arguments, *f* is 1/3 for a cylindrical morphology. The conductivity of PS-*b*-[PVBTMA][OH]-1.36 with lamellar structure and PS-*b*-[PVBTMA][OH]-1.19 is 12.55 S/cm (σ_{lam}) and 5.53 S/cm (σ_{cyl}), respectively, at fully hydrated state (90% RH and 80 °C). Derived from eq 1, the ratio of σ_{lam} to σ_{cyl} is equal to two times of the ratio of volume fraction of conducting block in these two samples. In this case, the ratio of σ_{lam} to σ_{cyl} (2.269) corresponds to twice the ratio of the mole fraction of the [PVBTMA][OH] (2.25) in PS-*b*-[PVBTMA][OH] samples with the assumption that the mole fraction is similar to the volume fraction of the conducting block because of undefined density of [PVBTMA][OH] at different RH levels and temperatures. With the same derivative, the *f* morphology factor for spherical morphology without well-defined orientation is found to be 1/3.

Different Relationship Between IEC and Conductivity at Low and High RH with Elevated Temperature

Conductivity data as a function of temperature of PS-*b*-[PVBTMA][OH] membranes at different humidity conditions are shown in Figure 6. The ionic conductivity of these samples increases with elevated temperature at humidity levels of 50, 70, and 90%. As shown in Figure 6(a), the conductivity at lower RH, that is, 50%, of PS-*b*-[PVBTMA][OH] increases with increasing IEC at temperature above 45 °C, which is the so-called refraction temperature, because there are more conductive groups in the membranes. However, the conductivity among these samples follows a reverse order at temperature below 45 °C and at 50% RH.

This unexpected behavior may result from the swelling and shrinkage of the [PVBTMA][OH] domain and the presence of

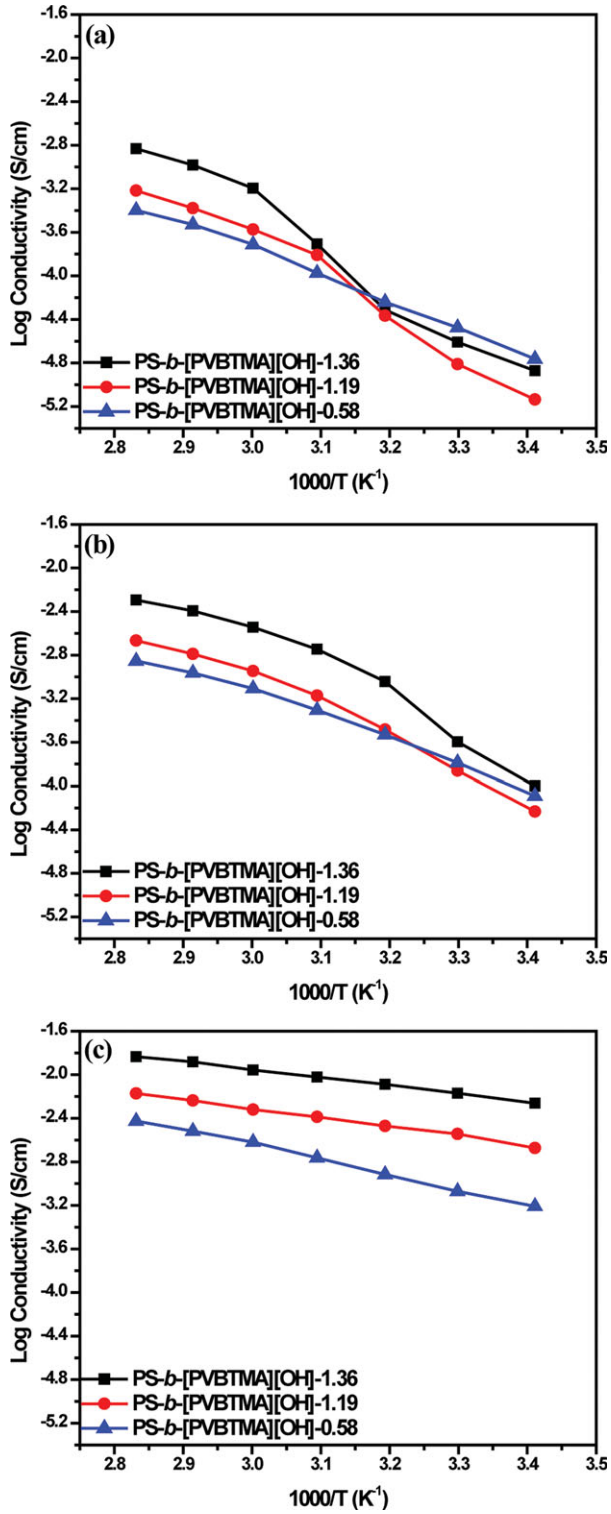

FIGURE 6 Temperature-dependent conductivity for PS-*b*-[PVBTMA][OH] membranes at (a) RH = 50%; (b) RH = 70%; and (c) RH = 90%.

grain boundaries within the microstructure. From the SAXS data of PS-*b*-[PVBTMA][OH] at RH = 50% at different temperatures 40, 50, and 60 °C [as shown in Fig. 4(a–c)], no morphological transition or changing of *d*-spacing happens for these samples. For the PS-*b*-[PVBTMA][OH]-1.36, which exhibit a lamellar morphology with a fixed and larger *d*-spacing (57.12 nm), the shrinkage of [PVBTMA][OH] block at low humidity and temperature and the appearance of grain boundaries (*T*-junctions) within the morphology reduce the effective conducting channels between two lamellar sheet leading to lower conductivity (shown in Scheme 2). As the temperature increases, the gradually swelling of [PVBTMA][OH] blocks magnify the effective conducting channels to generate a more well-connected conducting channel for ion transport. With the same arguments, this behavior is also observed for PS-*b*-[PVBTMA][OH]-1.19 samples with cylindrical morphology. Because the PS-*b*-[PVBTMA][OH]-0.58 sample likely exhibits a spherical morphology, the conductive channels are built by the stacking of spherical [PVBTMA][OH] domains. Because of the smaller *d*-spacing of PS-*b*-[PVBTMA][OH]-0.58 sample [31.42 nm, as shown in Fig. 4(c)], the conducting channels packed by stacking of spheres are already occupied by the [PVBTMA][OH] block at low humidity and temperature. Therefore, the swelling and shrinkage of the hydrophilic block have no significant effect on the conductivity. The refraction temperature at 70% humidity [35 °C, as shown in Fig. 6(b)] is lower than that at 50% humidity [45 °C, as shown in Fig. 6(a)] because more water swelling of the membrane at 70% humidity than at 50% humidity at a temperature below 45 °C facilitates ion transport. As shown in Figure 6(c), the conductivity of all three PS-*b*-[PVBTMA][OH] samples increases with increasing temperature and increasing IEC of the materials under fully hydrated conditions.

CONCLUSIONS

Block copolymers PS-*b*-[PVBTMA][OH] were synthesized by sequential monomer addition by ATRP of styrene followed by [VBTMA][BF_4] and then postpolymerization anion exchange from tetrafluoroborate to hydroxide counter anion. The disappearance of the characteristic stretching band of tetrafluoroborate anion from FTIR spectrum indicated the complete conversion of ion exchange. Microphase separation of the PS-*b*-[PVBTMA][BF_4] block copolymer into spherical,

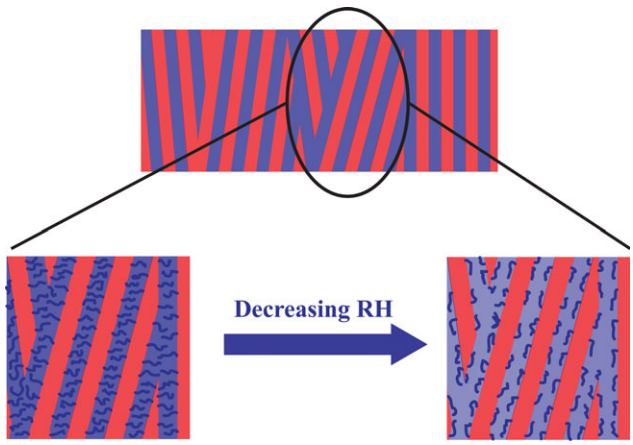

SCHEME 2 The proposed mechanism for ionic conductivity at low and high RH.

cylindrical, and lamellar microstructure was determined by SAXS. The investigation of humidity-dependent conductivity at 80 °C showed that the conductivity increases with increasing humidity at high humidity because of greater water uptake in the membrane-facilitating ion transport.

Additionally, the observation of nonlinearly increasing conductivity at RH = 90% with increasing IEC of the materials results from the inherent nature of the microstructures of the materials can be supported by a proposed theory.[48] The temperature-dependent conductivity at RH = 50, 70, and 90% showed that the ion conductivity of these three samples increases at elevated temperature. The conductivity of PS-*b*-[PVBTMA][OH] samples follows higher conductivity with higher IEC at temperatures above 45 °C at low humidity. The conductivity among these samples follows a reverse order at temperature below 45 °C at low humidity. This unexpected behavior may result from the differences of *d*-spacings in PS-*b*-[PVBTMA][OH] samples and different effects of swelling and shrinkage of [PVBTMA][OH] chain to conducting channels with lamellar, cylindrical, and spherical morphologies under low RH.

ACKNOWLEDGMENT

Funding was provided by the US Army MURI on Ion Transport in Complex Heterogeneous Organic Materials (W911NF-10-1-0520). Partial support was provided by the National Science Foundation Center for Hierarchical Manufacturing (CMMI-1025020) and an IGERT program (DGE-0504485). The use of Advanced Photon Source, an Office of Science User Facility operated for the US Department of Energy (DOE) Office of Science by Argonne National Laboratory, was supported by the US DOE under contract no. DE-AC02-06CH11357.

REFERENCES AND NOTES

1 L. Carrette, K. A. Friedrich, U. Stimming, *Fuel Cells* **2001,** *1*, 5–39.

2 B. C. H. Steele, A. Heinzel, *Nature* **2001,** *414*, 345–352.

3 D. E. Curtin, R. D. Lousenberg, T. J. Henry, P. C. Tangeman, M. E. Tisack, *J. Power Sources* **2004,** *131*, 41–48.

4 R. Borup, J. Meyers, B. Pivovar, Y. S. Kim, R. Mukundan, N. Garland, D. Myers, M. Wilson, F. Garzon, D. Wood, P. Zelenay, K. More, K. Stroh, T. Zawodzinski, J. Boncella, J. E. McGrath, M. Inaba, K. Miyatake, M. Hori, K. Ota, Z. Ogumi, S. Miyata, A. Nishikata, Z. Siroma, Y. Uchimoto, K. Yasuda, K.-I. Kimijima, N. Iwashita, *Chem. Rev.* **2007,** *107*, 3904–3951.

5 J. H. Reid, U.S. Patent 736,016, **1903**.

6 J. H. Reid, U.S. Patent 736,017, **1903**.

7 G. Erich, *J. Power Sources* **1996,** *61*, 99–104.

8 G. F. McLean, T. Niet, S. Prince-Richard, N. Djilali, *Int. J. Hydrogen Energy* **2002,** *27*, 507–526.

9 E. Gülzow, *Fuel Cells* **2004,** *4*, 251–255.

10 E. H. Yu, K. Scott, R. W. Reeve, *Fuel Cells* **2003,** *3*, 169–176.

11 C. Lamy, E. M. Belgsir, J. M. Léger, *J. Appl. Electrochem.* **2001,** *31*, 799–809.

12 A. V. Tripković, K. D. Popović, B. N. Grgur, B. Blizanac, P. N. Ross, N. M. Marković, *Electrochim. Acta* **2002,** *47*, 3707–3714.

13 M. A. Abdel Rahim, R. M. Abdel Hameed, M. W. Khalil, *J. Power Sources* **2004,** *134*, 160–169.

14 J. R. Varcoe, R. C. T. Slade, *Fuel Cells* **2005,** *5*, 187–200.

15 G. Couture, A. Alaaeddine, F. Boschet, B. Ameduri, *Prog. Polym. Sci.* **2011,** *36*, 1521–1557.

16 G. Merle, M. Wessling, K. Nijmeijer, *J. Membr. Sci.* **2011,** *377*, 1–35.

17 T. Sata, M. Tsujimoto, T. Yamaguchi, K. Matsusaki, *J. Membr. Sci.* **1996,** *112*, 161–170.

18 T. N. Danks, R. C. T. Slade, J. R. Varcoe, *J. Mater. Chem.* **2003,** *13*, 712–721.

19 H. Herman, R. C. T. Slade, J. R. Varcoe, *J. Membr. Sci.* **2003,** *218*, 147–163.

20 J. R. Varcoe, R. C. T. Slade, *Electrochem. Commun.* **2006,** *8*, 839–843.

21 M. R. Hibbs, M. A. Hickner, T. M. Alam, S. K. McIntyre, C. H. Fujimoto, C. Cornelius, *J. Chem. Mater.* **2008,** *20*, 2566–2573.

22 G. Wang, Y. Weng, D. Chu, R. Chen, D. Xie, *J. Membr. Sci.* **2009,** *332*, 63–68.

23 J. Wang, Z. Zhao, F. Gong, S. Li, S. Zhang, *Macromolecules* **2009,** *42*, 8711–8717.

24 J. Yan, M. A. Hickner, *Macromolecules* **2010,** *43*, 2349–2356.

25 N. J. Robertson, H. A. Kostalik, T. J. Clark, P. F. Mutolo, H. C. D. Abruña, G. W. Coates, *J. Am. Chem. Soc.* **2010,** *132*, 3400–3404.

26 B. Lin, L. Qiu, J. Lu, F. Yan, *Chem. Mater.* **2010,** *22*, 6718–6725.

27 B. Qiu, B. Lin, Z. Si, L. Qiu, F. Chu, J. Zhao, F. Yan, *J. Power Sources* **2012,** *217*, 329–335.

28 S. Gu, R. Cai, T. Luo, Z. Chen, M. Sun, Y. Liu, G. He, Y. Yan, *Angew. Chem. Int. Ed. Engl.* **2009,** *48*, 6499–6502.

29 J. Wang, S. Li, S. Zhang, *Macromolecules* **2010,** *43*, 3890–3896.

30 O. D. Thomas, K. J. W. Y. Soo, T. J. Peckham, M. P. Kulkarni, S. Holdcroft, *J. Am. Chem. Soc.* **2012,** *134*, 10753–10756.

31 B. Lin, L. Qiu, B. Qiu, Y. Peng, F. Yan, *Macromolecules* **2011,** *44*, 9642–9649.

32 Y. Luo, J. Guo, C. Wang, D. Chu, *J. Power Sources* **2010,** *195*, 3765–3771.

33 H. Xu, J. Fang, M. Guo, X. Lu, X. Wei, S. Tu, *J. Membr. Sci.* **2010,** *354*, 206–211.

34 A. K. Khandpur, S. Foerster, F. S. Bates, I. W. Hamley, A. J. Ryan, W. Bras, K. Almdal, K. Mortensen, *Macromolecules* **1995,** *28*, 8796–8806.

35 F. S. Bates, *Science* **1991,** *251*, 898–905.

36 Y. A. Elabd, E. Napadensky, C. W. Walker, K. I. Winey, *Macromolecules* **2006,** *39*, 399–407.

37 Y. A. Elabd, E. Napadensky, J. M. Sloan, D. M. Crawford, C. W. Walker, *J. Membr. Sci.* **2003,** *217*, 227–242.

38 T. J. Peckham, S. Holdcroft, *Adv. Mater. (Weinheim, Germany)* **2010,** *22*, 4667–4690.

39 M. J. Park, N. P. Balsara, *Macromolecules* **2009,** *43*, 292–298.

40 M. J. Park, K. H. Downing, A. Jackson, E. D. Gomez, A. M. Minor, D. Cookson, A. Z. Weber, N. P. Balsara, *Nanoletters* **2007,** *7*, 3547–3552.

41 M. J. Park, N. P. Balsara, *Macromolecules* **2008,** *41*, 3678–3687.

42 Y. A. Elabd, M. A. Hickner, *Macromolecules* **2010,** *44*, 1–11.

43 M. Tanaka, K. Fukasawa, E. Nishino, S. Yamaguchi, K. Yamada, H. Tanaka, B. Bae, K. Miyatake, M. Watanabe, *J. Am. Chem. Soc.* **2011,** *133*, 10646–10654.

44 J. Tang, H. Tang, W. Sun, H. Plancher, M. Radosz, Y. Shen, *Chem. Commun.* **2005,** 3325–3327.

45 J. Xia, K. Matyjaszewski, *Macromolecules* **1997,** *30*, 7697–7700.

46 U. Wendler, J. Bohrisch, W. Jaeger, G. Rother, H. Dautzenberg, *Macromol. Rapid Commun.* **1998,** *19*, 185–190.

47 M. Save, M. Manguian, C. Chassenieux, B. Charleux, *Macromolecules* **2004,** *38*, 280–289.

48 N. S. Wanakule, A. Panday, S. A. Mullin, E. Gann, A. Hexemer, N. P. Balsara, *Macromolecules* **2009,** *42*, 5642–5651.

49 J. Sax, J. M. Ottino, *Polym. Eng. Sci.* **1983,** *23*, 165–176.